IMAV2016-24
http://www.imavs.org/pdf/imav.2016.24

Improved Efficiency Electronic Speed Controller Development for 3-Phase Brushless DC Motor in Unmanned Aerial Systems

Kun Li*, Ao Chen, Kun Zhang and Ben M. Chen
Department of Electrical and Computer Engineering, NUS, Singapore, 117576

ABSTRACT

This paper presents the methodology and technique of implementing vector control method on brushless DC (BLDC) motors. Traditional scalar control method and the advanced field oriented control (FOC) are compared with the aspects of efficiency, control performance and reference speed range. Theoretical analysis of both methods are explained with their decomposed function components in detail. To obtain rotor position and its angular rate, a nonlinear observer based on the motor mathematical model is adopted to estimate these unknown states, for feedback to the control process. Customized hardware kit is designed and developed for implementation of the FOC algorithm. Several experiments are conducted to test the convergence speed, efficiency and reference speed range for both methods. The results show the superiority of FOC scheme with a properly tuned gain and parameter set.

1 INTRODUCTION

Brushless direct current (BLDC) motor has become one of the most popular motor types used in small-scaled electric vehicles, especially in the area of unmanned aerial systems (UAS). From 2003 to 2010, the BLDC motor market grew from $300 million to over $1.3 billion. Compared with brushed direct current (BDC) motors, BLDC motor shows a distinct advantage for its high control accuracy, long lifespan, high reliability, high power-to-volume ratio and low noise. When operated in rated conditions, the life expectancy is over 10,000 hours [1]. As a tradeoff, high control accuracy and reliability rely on the complexity of electrical speed controller (ESC) for BLDC motor.

The normal motor control techniques depend on the knowledge of accurate rotor position and some techniques require the feedback of rotational speeds. These techniques fall into two major categories: sensor feedback control and sensorless control [2, 3]. Sensor feedback control take in the sensor-measured angle and angular rate data as control feedbacks. These sensors providing the angle measurement include hall sensors, resolvers and encoders. For sensorless control, the normal method is to detect the back eletromagnetic force (BEMF) [4]. However, the BEMF signal is hard to detect, due to the electrical noise from the rotating machine, especially at low speed. The most common algorithm implemented in the commercial-off-the-shelf (COTS) ESC for BLDC motor is the scalar control method, also named six-step commutation scheme [5, 6]. However, according to the working principle, this method suffers from low efficiency caused by the copper loss. At low speed, the scalar control method is inaccurate due to its discrete nature and noise in BEMF detection [7]. Several research works proposed novel methods to detect the BEMF and improve the accuracy [8, 9], while efficiency is still a problem for scalar control method.

The field oriented control (FOC) is a vector control technique which was first conceptualized in 1929 by Robert H.Park [10]. FOC technique [11, 12] maximizes the quadrature current component and minimizes direct current component, in order to produce constant torque effectively. It is originally designed for permanent magnetic synchronous motors (PMSMs). Some researchers [13] even extended this advanced control technique for BLDC (with trapezoidal BEMF compared to sinusoidal BEMF for PMSMs). However, due to the difference between 3-phase AC machine and BLDC, the BEMF method cannot be directly implemented for FOC technique, and rotor position needs to be observed for sensorless control method.

This research work mainly focuses on the development of a FOC control hardware kit and the implementation of the vector control scheme based on the algorithm workflow. Section 2 gives the general mathematical model of a 3-phase BLDC. Section 3 gives the comparison between the traditional scalar control method and vector control method FOC. Section 4 gives the algorithm implementation details and the hardware overview. Followed by the experimental setup in Section 5 and results are discussed in Section 6.

2 GENERAL BLDC MOTOR MODEL

Fig. 1 gives a general synchronous motor model, namely the BLDC type or 3-phase AC type, controlled by a logically designed invertor network. Each phase is controlled by two electrical switches, i.e. power metaloxidesemiconductor field-effect transistors (MOSFETs) shown as T_i in Fig. 1, one terminal of which connects to power E and the other terminal connects to power ground G.

The mathematical model can be described as a differential equation with constant coefficients with applying the Lenz-

*Email address: elelik@nus.edu.sg

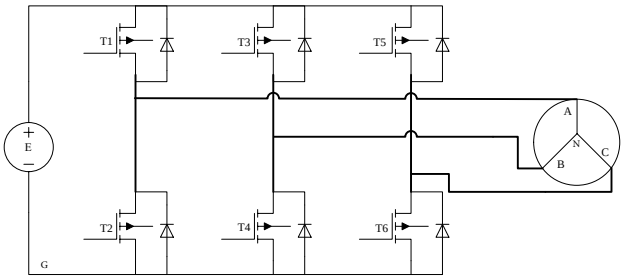

Figure 1: Closed-loop controller architecture of a BLDC ESC module.

Faraday model as follows:

$$\begin{bmatrix} v_a \\ v_b \\ v_c \end{bmatrix} = R_s \begin{bmatrix} i_a \\ i_b \\ i_c \end{bmatrix} + \frac{d}{dt} \begin{bmatrix} L_s & M & M \\ M & L_s & M \\ M & M & L_s \end{bmatrix} \begin{bmatrix} i_a \\ i_b \\ i_c \end{bmatrix} + \frac{d}{dt} \begin{bmatrix} \Phi_{\text{sf}} \cos(\theta) \\ \Phi_{\text{sf}} \cos(\theta - \frac{2\pi}{3}) \\ \Phi_{\text{sf}} \cos(\theta + \frac{2\pi}{3}) \end{bmatrix} \quad (1)$$

where R_s and L_s are the stator resistance and inductance, M is the mutual inductance between two stators, $[v_a \ v_b \ v_c]^T$ and $[i_a \ i_b \ i_c]^T$ are stator voltage and current, θ is the rotor position and for a multi-pole BLDC, the rotor position θ is calculated from the electrical angle θ_e with $\theta = 2\theta_e/N_p$, where N_p is the number of pole pairs. Φ_{sf} is the max flux value created by the permanent magnet through the stators.

3 Scalar Control Method

COTS ESCs are implemented with the most direct method to control the rotor motion, scalar control [14, 15]. Each conducting interval is 120° by electrical angle, which is exactly 120° by mechanical rotating angle for a single pole-pair permanent magnet rotor.

Fig. 2 shows the control waveform of the six-step commutation and the sequence is as AB-AC-BC-BA-CA-CB to make sure that magnetic field generated by the winding keeps changing 60° each commutation step, yielding a constant rotating direction. The core technology inside is the knowledge of the rotor position, i.e. the exact sector the rotor currently lies in. The technique normaly uses the third floating phase to detect the BEMF [16, 17]. This is the voltage generated in BLDC motors when there is relative motion between the armature of the motor and the magnetic field from the motor's field magnets, or windings. Further, the voltage is proportional to the magnetic field, length of wire in the armature, and the speed of the motor according to Faraday's law.

As it is difficult to obtain the neutral voltage of a three-phase BLDC motor, which is often built in the mechanical structure. In the practical case, a virtual neutral point resistance network is built to emulate the motor neutral point for

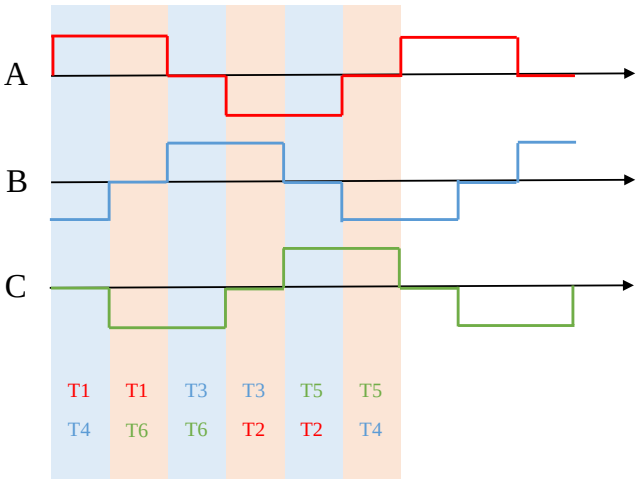

Figure 2: Six-step commutation control waveforms.

zero-crossing BEMF detection [14]. As such, the timing of commutation sequence is obtained via measuring the zero-crossing BEMF of the floating terminal.

4 Vector Control Method

FOC is commonly used for PMSM motor, and has not been commercially applied on BLDC motor. According to the model provided by Eq. 1, the rotational motion is created by the force exerted by the magnetic fields from stator and rotor. Since the rotor's magnetic field is fixed, the way of exerting stator magnetic field determines the performance and efficiency of the rotation. By properly aligning the rotor and stator flux, the most optimal torque production of the rotor is generated by vector control method [18].

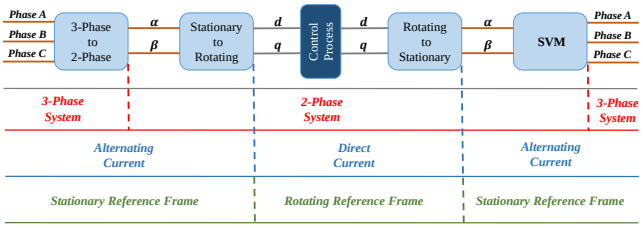

Figure 3: Process of FOC.

As shown in Fig. 3, the process of FOC can be modularized into five blocks. The first block is conversion of stator winding current or voltage from 3-phase rotating coordinate (a, b, c) to 2-phase rotating coordinate (α, β), also known as Clarke transformation, in order to reduce the control complexity. The projection into the 2-phase coordinate system depending on time and rotational speed:

$$\begin{aligned} i_{S\alpha} &= i_a \\ i_{S\beta} &= \frac{1}{\sqrt{3}} i_a + \frac{2}{\sqrt{3}} i_b \end{aligned} \quad (2)$$

where the model in Eq. 1 can be rewritten in the 2-phase rotating frame $(\alpha,\ \beta)$ as,

$$l_s\dot{i}_{\alpha\beta} = -r_s i_{\alpha\beta} + \omega\Phi_{\text{sf}} \begin{bmatrix} \sin\theta \\ \cos\theta \end{bmatrix} + v_{\alpha\beta} \tag{3}$$

where $l_s = 3/2L_s$ and $r_s = 3/2R_s$.

The second block is a transformation from time-variant system $(\alpha,\ \beta)$ to a time-independent system direct-quadrature $(d,\ q)$, also known as Park transformation. The d-axis is aligned with the rotor flux and the q-axis is orthogonal to the rotor flux. The core of the Park transformation is the feedback of the rotor position θ, with which the current can be transformed into flux and torque components with the following equations:

$$\begin{aligned} i_{Sd} &= i_{S\alpha}\cos\theta + i_{S\beta}\sin\theta \\ i_{Sq} &= -i_{S\alpha}\sin\theta + i_{S\beta}\cos\theta \end{aligned} \tag{4}$$

The third block is the control process component regarding with the decoupled time-invariant system. In this paper, a simple PI controller was implemented for both the speed and torque component. The forth block is formulation of the control outputs. Control output generated from the speed and torque controller are then fed to the reverse Park transformation as:

$$\begin{aligned} v_{ref\alpha} &= v_{refd}\cos\theta - v_{refq}\sin\theta \\ v_{ref\beta} &= v_{refd}\sin\theta + v_{refq}\cos\theta \end{aligned} \tag{5}$$

Ideally the current vector should always be in the quadrature direction of the rotor and rotate together with the rotor. In this case, constant torque can be produced efficiently [7, 19].

The last block is to generate actuator signal to the 3-phase invertors, namely space vector modulation (SVM). SVM is a method to generate pulse width modulation (PWM) to control the timing of the commutation. There will be two considerations of the MOSFET switches as: a) three of the switches must be ON and the other three must be OFF; b) the high and the low side switches of the same phase must be driven with two complementary pulsed signals. Under these constraints, there will be eight combinations which forms six sectors of the whole loop.

As state above, knowledge of the rotor position is the core of BLDC motor control, especially in vector control method, where a slight error in rotor position will bring large deviation in d-q axis estimation. However, due to limitations of the applications in UAS on the aspects of weight and cost budgets, sensorless control of the BLDC is considered instead of using resolvers or encoders. Research works in [20, 21] provide us a solution to estimate rotor position and rotational speed with a nonlinear observer. Consider the model in $(\alpha,\ \beta)$ frame, a new state variable is defined as,

$$x = l_s i_{\alpha\beta} + \Phi_{\text{sf}} \begin{bmatrix} \cos\theta \\ \sin\theta \end{bmatrix} \tag{6}$$

$$y = -r_s i_{\alpha\beta} + v_{\alpha\beta} \tag{7}$$

where we have simply as $\dot{x} = y$ according to the model in Eq. 3. A vector function is defined to construct the nonlinear observer,

$$\eta(x) = x - l_s i_{\alpha\beta} \tag{8}$$

and we have the Euclidean norm of the vector function as $||\eta(x)||^2 = \Phi_{\text{sf}}^2$. The nonlinear observer is constructed as:

$$\dot{\hat{x}} = y + \frac{\kappa}{2}\eta(\hat{x})\left[\Phi_{\text{sf}}^2 - ||\eta(\hat{x})||^2\right] \tag{9}$$

where $\hat{x}$ is the observer state variable and $\kappa > 0$ is the observer gain. According to the state expression in Eq. 6, we have,

$$\begin{bmatrix} \cos\hat{\theta} \\ \sin\hat{\theta} \end{bmatrix} = \frac{1}{\Phi_{\text{sf}}}(\hat{x} - l_s i_{\alpha\beta}) \tag{10}$$

and we can obtain the estimate of the rotor position as,

$$\hat{\theta} = \tan^{-1}\left(\frac{\hat{x}_2 - l_s i_\beta}{\hat{x}_1 - l_s i_\alpha}\right) \tag{11}$$

and thus an observer error can be further obtained as,

$$\begin{aligned} \dot{\tilde{x}} &= -\kappa\alpha(\tilde{x},t)\left\{\tilde{x} + \Phi_{\text{sf}}\begin{bmatrix} \cos\theta(t) \\ \sin\theta(t) \end{bmatrix}\right\} \\ \alpha(\tilde{x},t) &= \frac{1}{2}||\tilde{x}||^2 + \Phi_{\text{sf}}[\tilde{x}_1\cos\theta(t) + \tilde{x}_2\sin\theta(t)] \end{aligned} \tag{12}$$

where $\alpha(\tilde{x},t)$ is the cost function to evaluate the stability properties. The stability proof and construction of the speed observer can be referred in [20, 21].

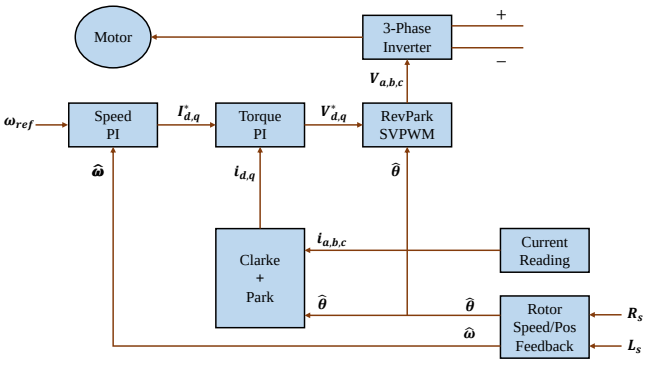

Figure 4: Overview of the FOC control logics.

The whole workflow of the FOC process is explained in Fig. 4. The startup procedure depends on an alignment or pre-position phase to check if the angle and rotational speed estimator are able to converge. For BLDC motor, the torque produced is not relevant with direct component, hence the reference i_{refd} can be set to zero for optimal performance. Several parameters are recursively tuned to achieve the best performance, such as startup duration, etc. These parameters significantly affect the dynamic performance of rotor.

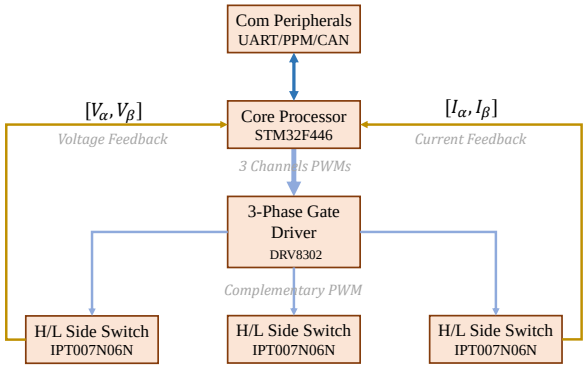

Figure 5: FOC hardware development: function blocks incorporated.

5 Hardware and Experiments

According to the process components analyzed in Fig. 3, function blocks need to be incorporated are listed in Fig. 5 with the signal flows. Communication peripherals are reserved for the upper-level command from the UAS avionic system, with protocols of serial or controller area network (CAN) bus or PWM signals. The processor used is STM32F446 with ARM Cortex-M3 core with a real-time operating system (RTOS)[1] running on. An device DRV8302 is used for 3-phase gate driving and process the measured phase current. The layout of the board can be seen in Fig. 6.

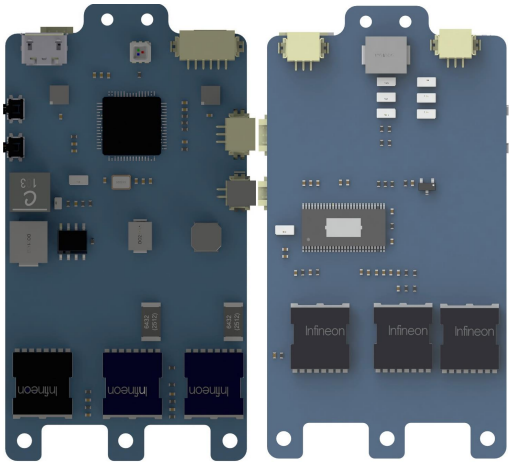

Figure 6: FOC hardware development: printed circuit board (PCB) overview.

An experiment is designed to verify the advantages in control performance and efficiency for BLDC compared with the traditional ESCs (here we use a T-motor ESC as a comparison). BLDC motors (hexTronik outrunner 1700 kV and BR 2804 − 1800 kV) with 6030 propeller load is mounted on ATI load cell Mini40 for force and torque measurement. Eagle-tree elogger v4 testing suite is used for the recording of rotational speed, overall voltage, current assumption and temperature information. Efficiency η can be calculated as equation below, where τ is the torque produced by the propeller,

$$\eta = \frac{2\pi\omega\tau}{60 \times vi} \tag{13}$$

[1]ChibiOS: please refer http://www.chibios.org/dokuwiki/doku.php for more information.

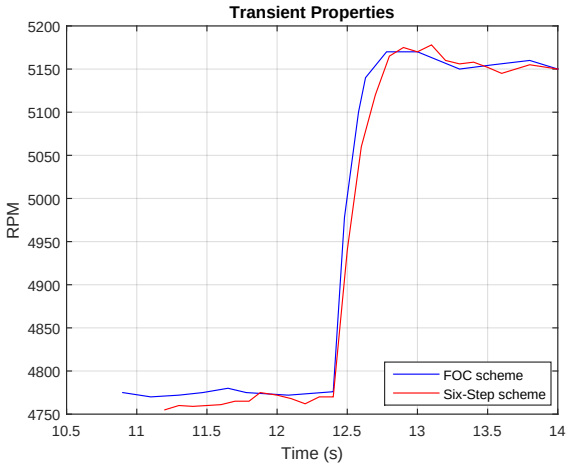

Figure 8: Dynamic response of FOC/SixStep with changing reference speed for rotor combo of hexTronik outrunner 1700 kV and 6030 propeller.

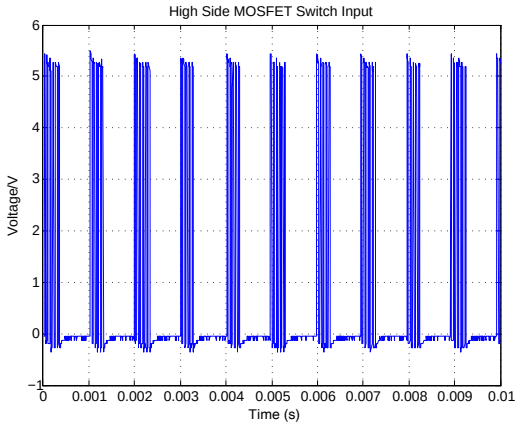

Figure 7: High side switching input with reference speed of 1500 RPM for rotor combo of hexTronik outrunner 1700 kV and 6030 propeller.

6 Results and Discussions

The same reference speed from 4750 RPM to 5150 RPM was fed to the traditional ESC set as well as the FOC board with the PID parameters recursively tuned. The FOC scheme

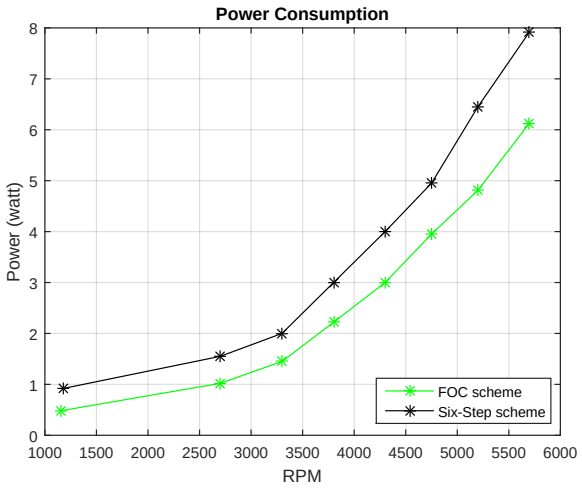

Figure 9: Power consumed by the motor under different speed for rotor combo of hexTronik outrunner 1700 kV and 6030 propeller.

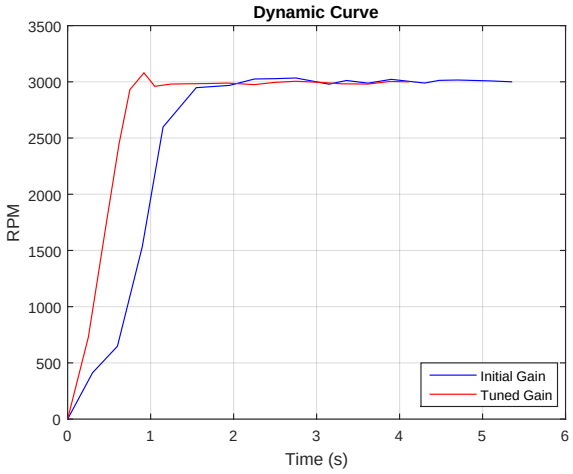

Figure 11: Start up process with a reference speed of 3000 RPM with hexTronik outrunner 1700 kV and 6030 propeller.

shows a faster convergent period around 0.4 s compared to the six-step method. During the startup phase, the controller ramps up from zero to reference speed with a pre-positioning algorithm to achieve alignment. This is used to make sure the initial rotor position and check the reliability of rotor position and speed estimator.

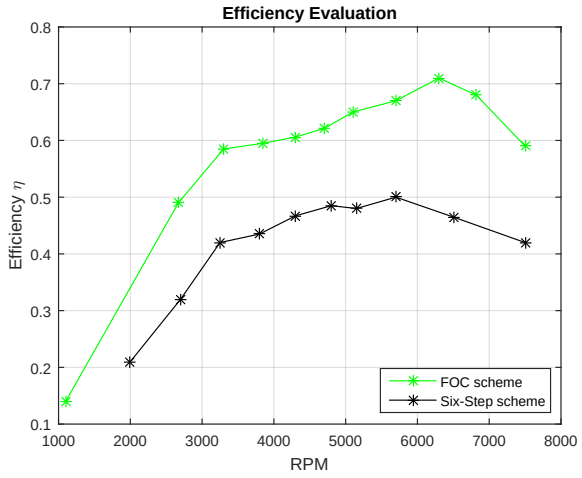

Figure 10: Efficiency evaluated at different rotating speed for rotor combo of BR 2804 − 1800 kV and 6030 propeller.

Fig. 7 gives the signal generated from the module SVPWM to drive for the 3-phase invertor. As shown from the graph, the duty cycle of the PWM signal is updated each loop to adjust the vector during different sectors of SVM. High efficiency is the core advantage of FOC among other motor control techniques, which is shown in Fig. 9 and Fig. 10 respectively. Fig. 9 gives the data plot in power consumption form for the rotor set hexTronik outrunner 1700 kV. Fig. 10 gives calculated efficiency with the same rotor set under FOC and six-step algorithm separately. Under different reference speed, the efficiency of FOC controller is about 15% higher than commercial six-step controller.

As we can see, another significant advantage of FOC controller among other commercial scalar control ESCs is the ability to maintain stable control at low speed reference. The experiment in Fig. 11 reveals that the FOC controller is able to maintain both motors at low reference speed and deliver significant torque at the same time. On the other hand, commercial controller cannot drive both BLDC motor to speed below 2000 RPM, compared to the performance of FOC scheme, which is indicated in the ramp-up process in Fig. 11. This is because the BEMF zero crossing detection method used in six-step algorithm is not accurate due to the electrical noise, especially at low commutation speed.

As current hardware setup does not support real-time measurement log file to record current and voltage, observation of measurements is from oscilloscope and external devices for rotational speed and torque. Thus it is impractical to identify an accurate dynamic model for model-based control. PI gains are tuned for both speed and torque loop based on the performance we have recorded, i.e., the overshoot and settling time.

7 Conclusion

This paper presented the development of a vector control method for BLDC motor and implementation of FOC control algorithm. Each core component of FOC algorithm is detailed with specific explanation of the rotor position and speed estimation with a nonlinear observer. The hardware system to implement the FOC algorithm is built from scratch. From the experiment results, the vector control method out-

weighs the traditional scalar control method in the aspects of dynamic performance, transient properties, efficiency in power consumption and low reference speed control. In the next phase, we will identify an accurate dynamic model of the rotor system for implementation of a model-based control. More experiments will be done to verify the robustness and efficiency of the FOC method with long endurance tests and different rotor loads before integration into the UAS in the future.

REFERENCES

[1] P. Yedamale. Brushless DC (BLDC) motor fundamentals. *Microchip Technology Inc*, 20:3–15, 2003.

[2] Z. Chen, M. Tomita, S. Doki, and S. Okuma. An extended electromotive force model for sensorless control of interior permanent-magnet synchronous motors. *IEEE transactions on Industrial Electronics*, 50(2):288–295, 2003.

[3] T. H. Kim and M. Ehsani. Sensorless control of the bldc motors from near-zero to high speeds. *IEEE Transactions on Power Electronics*, 19(6):1635–1645, 2004.

[4] F. Genduso, R. Miceli, C. Rando, and G. R. Galluzzo. Back emf sensorless-control algorithm for high-dynamic performance pmsm. *IEEE Transactions on Industrial Electronics*, 57(6):2092–2100, 2010.

[5] J. Holtz, W. Lotzkat, and A. M. Khambadkone. On continuous control of PWM inverters in the overmodulation range including the six-step mode. *IEEE Transactions on Power Electronics*, 8(4):546–553, 1993.

[6] M. A. Abbas, R. Christen, and T. M. Jahns. Six-phase voltage source inverter driven induction motor. *IEEE Transactions on industry applications*, (5):1251–1259, 1984.

[7] N. Matsui and M. Shigyo. Brushless DC motor control without position and speed sensors. In *Industry Applications Society Annual Meeting, 1990., Conference Record of the 1990 IEEE*, pages 448–453. IEEE, 1990.

[8] J. Shao, D. Nolan, and T. Hopkins. A novel direct back EMF detection for sensorless brushless DC (BLDC) motor drives. In *Applied Power Electronics Conference and Exposition, 2002. APEC 2002. Seventeenth Annual IEEE*, volume 1, pages 33–37. IEEE, 2002.

[9] W. Zhao, M. Cheng, W. Hua, H. Jia, and R. Cao. Back-EMF harmonic analysis and fault-tolerant control of flux-switching permanent-magnet machine with redundancy. *IEEE Transactions on Industrial Electronics*, 58(5):1926–1935, 2011.

[10] R. H. Park. Two-reaction theory of synchronous machines generalized method of analysis-part i. *Transactions of the American Institute of Electrical Engineers*, 48(3):716–727, 1929.

[11] I. Takahashi and T. Noguchi. A new quick-response and high-efficiency control strategy of an induction motor. *IEEE Transactions on Industry applications*, (5):820–827, 1986.

[12] R. Gabriel, W. Leonhard, and C. J. Nordby. Field-oriented control of a standard AC motor using microprocessors. *IEEE transactions on industry applications*, (2):186–192, 1980.

[13] J. P. John, S. S. Kumar, and B. Jaya. Space vector modulation based field oriented control scheme for brushless DC motors. In *Emerging Trends in Electrical and Computer Technology (ICETECT), 2011 International Conference on*, pages 346–351. IEEE, 2011.

[14] J. Shao. *Direct back EMF detection method for sensorless brushless DC (BLDC) motor drives*. PhD thesis, Virginia Polytechnic Institute, 2003.

[15] J. Shao, D. Nolan, M. Teissier, and D. Swanson. A novel microcontroller-based sensorless brushless DC (BLDC) motor drive for automotive fuel pumps. *Industry Applications, IEEE Transactions on*, 39(6):1734–1740, 2003.

[16] D. M. Erdman. Control system, method of operating an electronically commutated motor, and laundering apparatus, March 31 1987. US Patent 4,654,566.

[17] K. Iizuka, H. Uzuhashi, M. Kano, T. Endo, and K. Mohri. Microcomputer control for sensorless brushless motor. *Industry Applications, IEEE Transactions on*, (3):595–601, 1985.

[18] G. N. Mahesh, Y. Kiran, and D. Parthasarthy. Modelling of buck DC-DC converter using simulink. *International Journal of Innovative Research in Science Engineering and Technology*, 3(7):14965–14975, 2014.

[19] L. Hoang. Comparison of field-oriented control and direct torque control for induction motor drives. In *Industry Applications Conference, 1999. Thirty-Fourth IAS Annual Meeting. Conference Record of the 1999 IEEE*, volume 2, pages 1245–1252. IEEE, 1999.

[20] R. Ortega, L. Praly, A. Astolfi, J. Lee, and K. Nam. Estimation of rotor position and speed of permanent magnet synchronous motors with guaranteed stability. *IEEE Transactions on Control Systems Technology*, 19(3):601–614, 2011.

[21] J. Lee, J. Hong, K. Nam, R. Ortega, L. Praly, and A. Astolfi. Sensorless control of surface-mount permanent-magnet synchronous motors based on a nonlinear observer. *IEEE Transactions on power electronics*, 25(2):290–297, 2010.